JOURNAL OF PROPULSION AND POWER
Vol. 11, No. 5, September–October 1995

# Approach to In Situ Analysis of Scramjet Combustor Behavior

William O. T. Peschke*
*United Technologies Research Center, East Hartford, Connecticut 06108*

**Procedures used to assess combustion behavior of scramjet engines in the 1960s were not published at that time, but may be relevant to current scramjet research. This article describes hydrogen-fueled scramjet investigations performed at the General Applied Science Laboratories during the 1966–1970 time period. The analysis procedure, involving fuel-injection tailoring, aided in locating injection sites in the scramjet combustor and in predicting the pressure rises induced by combustion at selected points in the combustor. The method was applied to two geometrically dissimilar engines whose performance levels were measured in similar freejet facilities. One of these engines incorporated a combustor entrance (gap) height of approximately 2.9 in. and an overall combustor/nozzle length of 10 gap heights. The injector placement resulting from this development approach did not induce pressure distributions that one would associate with the higher-process-efficiency, minimum-entropy solution. Nevertheless, approximately 80% of the target thrust levels were attained in these engines at fuel–air equivalence ratios of one, without the benefit of isolators and without deleterious combustor–inlet interactions. Agreement between predicted and measured combustion pressure rises was generally good and satisfactory agreement exists between the pressure rise measured and that calculated using a current cycle analysis.**

## Nomenclature

$A$ = area, in.$^2$
$D$ = injector orifice diameter, in.
*Eta-c* = combustion efficiency
$F$ = net thrust, lbf
$G$ = combustor throat (gap) height, in.
$L$ = length, in.
$M$ = Mach number
$P$ = pressure, psia
$u$ = velocity, fps
$W$ = weight flow rate, lbm/s
$x$ = streamwise distance, in.
$\lambda$ = mass flux ratio, $\rho_j u_j/\rho_e u_e$
$\rho$ = density, lbm/ft$^3$
$\phi$ = fuel–air equivalence ratio

*Subscripts*
$e$ = airflow (external to jet)
$j$ = jet (fuel) flow

## Introduction

A PROGRAM involving the General Applied Science Laboratories (GASL), at the time a subsidiary of The Marquardt Corporation, was initiated in April 1965, and had as its objective the demonstration of useful thrust development from a scramjet engine in flight. The Scramjet Incremental Flight Test Program[1] was administered by the Air Force Aero Propulsion Laboratory. A nonpowered configuration of the test vehicle was flown to acquire aerodynamic and instrumentation data in January 1967. The remaining flight tests of the program were cancelled in August 1967, prior to the completion of the ground development of the scramjet engine.

Early testing of the integrated inlet–combustor configuration was performed in a uniform Mach 5 flowfield to confirm the three-dimensional, thermal compression features of the engine design. In subsequent tests performed in a conical flowfield that simulated the flow produced by a vehicle forebody, local flow separation problems in the test model persistently resulted in unstart during combustion. This occurrence prevented the attainment of satisfactory combustor operation at equivalence ratios exceeding approximately 0.4. Tests in a modified model were conducted using a tailored fuel injection distribution and resulted in satisfactory combustion and thrust performance at fuel–air equivalence ratios on the order of unity.

Based on the measured wall static pressure distribution, the combustor flow in this device remained supersonic during combustion, even at equivalence ratios approaching one. It is true that, in general, for combustor entrance Mach numbers corresponding to flight at a Mach number of 8 or below, combustion in a constant area duct or in a duct with minimal wall divergence results in high local pressure rises that induce the occurrence of strong precombustion shock waves. This is particularly so when the fuel is introduced from the duct wall in a direction normal to the combustor airflow. As a consequence of the effects of this process, local separation of the flow may occur and, for moderately small channels, the bulk flow Mach number approaches 1. Thus, at any axial location in the flow, the static pressure measured across the flow is essentially constant. In the combustor discussed herein, the upper and lower wall static pressures at a given axial location were not equal.

The combustion process observed in this combustor development effort was thus a demonstration of the diffusive mixing and burning process described by Ferri.[2] One may attribute the wall static pressure characteristics of this device 1) to the use of streamwise fuel injection and 2) to the complimentary interrelationship between the heat release and the flow area distributions. As such, in accordance with the proposition set forth by Anderson et al. in Ref. 3, the flowfield characteristics in the subject combustor may be similar to those that are expected to characterize hypersonic combustion.

## Engine/Vehicle Concept

The engine/vehicle concept, reproduced in Fig. 1 from Ref. 1, comprised a finned, axisymmetric body incorporating a conical forebody and a tapered, cylindrical afterbody. The

Presented as Paper 93-2328 at the AIAA/SAE/ASME/ASEE 29th Joint Propulsion Conference, Monterey, CA, June 28–30, 1993; received Dec. 4, 1993; revision received Oct. 21, 1994; accepted for publication Nov. 3, 1994. 

*Senior Research Engineer, Advanced Propulsion.

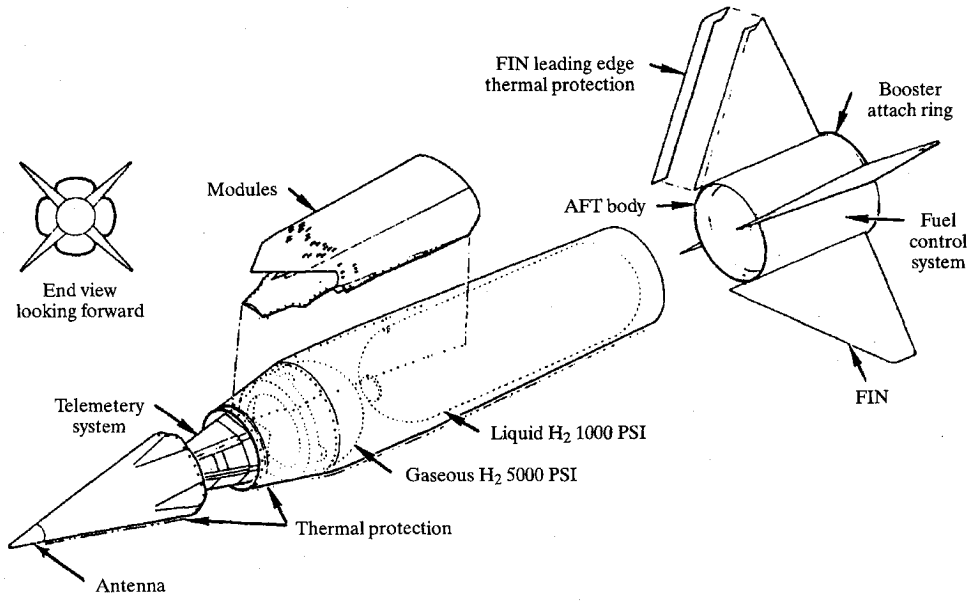


**Fig. 1 Scramjet Incremental Flight Test Vehicle (IFTV).[1]**

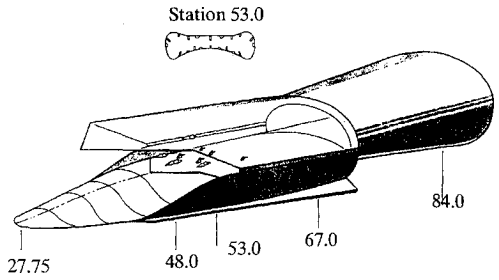


Note: Showing lower injectors only
(Units in inches)

**Fig. 2 Scramjet engine module.[1]**

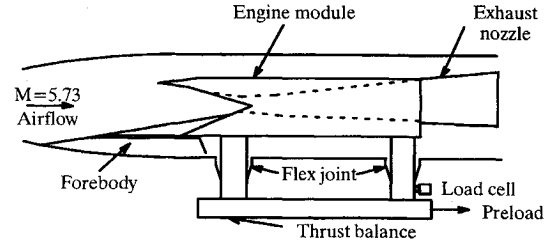


**Fig. 3 Freejet installation of engine module.**

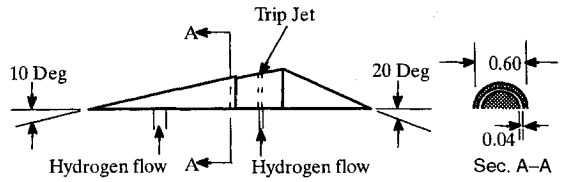


**Fig. 4 Primary (pilot) fuel injector.**

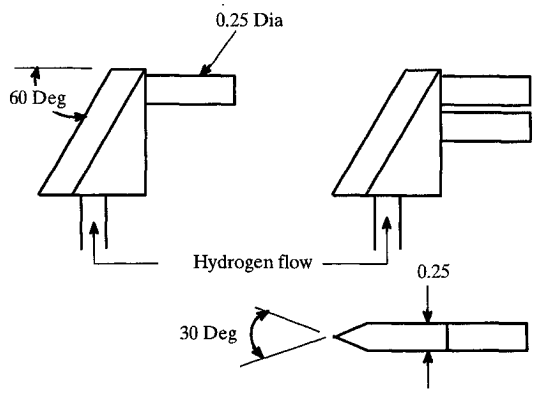


**Fig. 5 Secondary strut fuel injectors.**

propulsion system consisted of four scramjet modules installed symmetrically around the vehicle body as shown in the figure. This vehicle was to be boosted to an altitude of approximately 56,000 ft and to a velocity of approximately 5400 fps to enable scramjet takeover to occur. The scramjets were to increase the flight velocity a minimum of 600 fps to at least 6000 fps.

## Engine Module Description

One of the scramjet engine modules is shown in Fig. 2. A cross section through the flow passage at the combustor entrance is shown in the inset. The station numbers in the diagram correspond to the distance, in inches, from the nose of the flight vehicle. A full-scale, heavyweight version of this engine was tested while suspended on a thrust balance in a freejet tunnel as shown in Fig. 3. To provide a simulation of the flowfield that would be developed by the conical forebody of the flight vehicle, an extension of the inlet ramp, affixed to the floor of the tunnel, was used. Pertinent geometric characteristics of the engine were as follows:

| | | |
|---|---|---|
| freestream capture area $A_0$ | = | 94.0 in.$^2$ |
| combustor entrance area $A_2$ | = | 24.2 in.$^2$ |
| combustor exit area $A_4$ | = | 47.0 in.$^2$ |
| nozzle exit area $A_6$ | = | 108.0 in.$^2$ |
| combustor (gap $G$) height at throat | = | 2.92 in. |
| combustor width at throat | = | 10.3 in. |
| combustor length/gap $L_4/G$ | = | 4.8 |
| combustor + nozzle length/gap $L_6/G$ | = | 10.6 |

The combustor entrance was coincident with the inlet exit and comprised a minimum cross section that was swept back at an angle of approximately 50 deg on the body (ramp) side and approximately 64 deg on the cowl side. The primary or pilot fuel injectors were as shown in the schematic diagram of Fig. 4, excerpted from Ref. 4, and were designed to deliver room temperature, gaseous hydrogen at sonic velocity through the 0.04-in.-wide annular slot shown in the figure. A normal

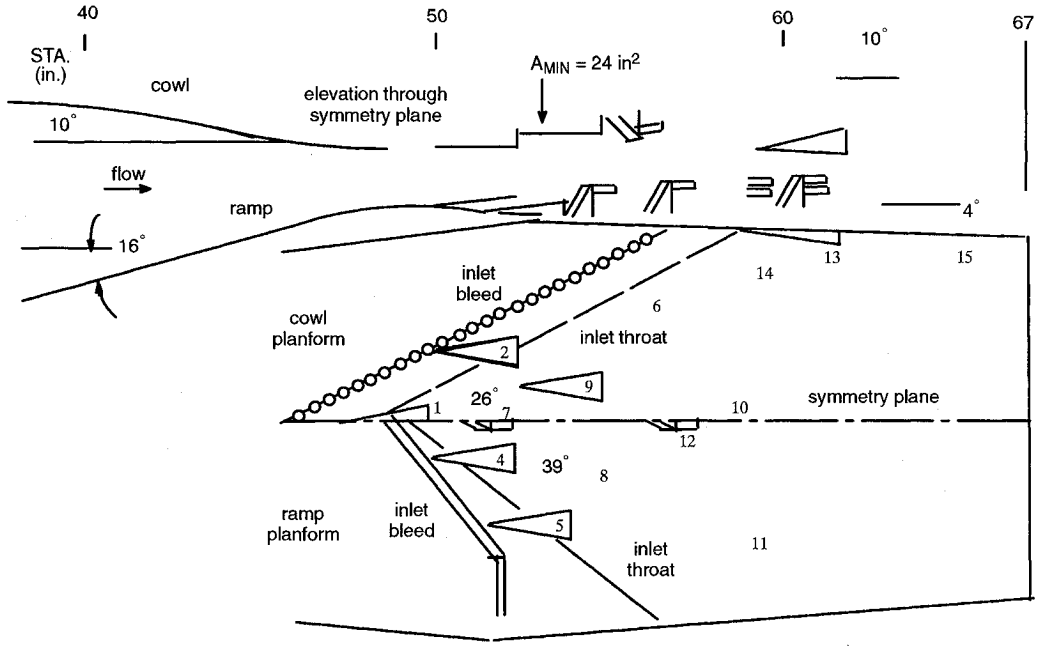


**Fig. 6 Internal lines and fuel injector locations.**

"trip" jet was also incorporated as shown. Small, strut-type fuel injectors incorporating 0.25-in.-diam tubes, oriented so as to introduce the hydrogen in a streamwise manner, but above the surface as shown in Fig. 5 (Ref. 4), were used as secondary injectors. A schematic diagram, showing the internal lines of the engine module and the fuel injector placement, is shown in Fig. 6.

## Experimental Program

The experimental development of the supersonic combustor was accomplished in a freejet tunnel that was provided with air from a vitiated-air heater. The heater burned hydrogen in air to which oxygen was added to provide an oxygen mole fraction equal to that of atmospheric air. The supersonic airflow was delivered to the model at a Mach number of 5.73 and the heater total pressure and temperature were 700 psia and 2700°R, respectively. The thrust balance comprised a pair of horizontal steel beams that supported the engine module in the tunnel and were suspended from overhead.

Engineering models were specified to permit a study of the effects of fuel injection and combustion on the wall static pressure field within the supersonic combustor. A shock wave–boundary-layer interaction model was adopted to provide indications of incipient boundary-layer separation. It was assumed that the failure to achieve a predicted local static pressure rise was related to a local combustion inefficiency. The regions affected by the combustion of fuel were identified by calculating the geometry of the shock wave induced by the "thermal-compression" process and graphically locating its intersection with the interior surface of the combustor.

### Combustor Evolution

A simple geometric analysis using an assumed jet spreading angle of 4 deg (half-angle) was applied to estimate the dispersal of fuel that could be achieved at the combustor exit cross section at an assumed pilot–hydrogen flow rate. The use of a 4-deg half-angle was based on earlier data acquired in separate single-injector experiments using hydrogen. A total of seven conical pilot injectors was installed, viz., three at the cowl throat and four at the ramp throat, as shown in Fig. 6 and in the photograph of Fig. 7. The relative locations of all fuel injectors, projected on Station 58, are depicted in the diagram on the left in Fig. 8. The two sets of pilots were interdigitated. Referring to Fig. 6, e.g., pilot injector 1 was

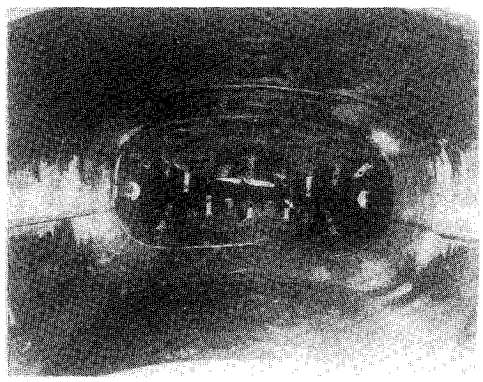

**Fig. 7 View of combustor from nozzle exit.**

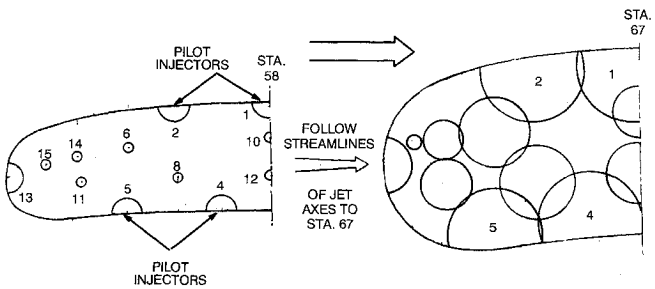


**Fig. 8 Fuel injector sites projected on Station 58 cross section and fuel jet disposition at Station 67. (Numerals correspond to fuel injectors shown in Fig. 6.)**

situated on the line of symmetry of the cowl while pilot injector 2 was centered on a line that bisected the distance between ramp-pilot injectors 4 and 5. Pilot injector 9, which was added to the set of pilot injectors during the sequence of experiments, was similarly placed approximately halfway between injectors 1 and 2. The estimated geometry of the regions fueled by the pilots and the strut fuel injectors, at the combustor/nozzle interface (Station 67) is shown on the right in Fig. 8. The geometry of the fueled regions was estimated graphically under the questionable assumption that the fuel-jet axis "followed" the contour of the wall to which the in-

jector was affixed. This assumption disregards the effects of interactions between the fuel jets and the shock waves in the relatively short combustor. With only the seven pilot fuel injectors installed, the model, which incorporated a substantial number of wall static pressure taps, was placed in the freejet tunnel for testing. The effect on the wall static pressure levels induced by the combustion of hydrogen at various flow rates was recorded and compared with a simple analysis, discussed below, to estimate the quantity of hydrogen burned. For the experiments discussed here, the initial centerline flow conditions on the ramp side at the inlet throat were as follows: Mach number, 3.55; static pressure, 4.0 psia; and static temperature, 878°R.

By virtue of the configuration of the inlet, the centerline conditions on the cowl side were slightly different, i.e., the throat Mach number was 3.82 and the static pressure was 3.50 psia. Owing to the presence of the 10-deg conical pilot fuel injector, the ramp-side flow conditions existing at the fuel injection location, i.e., the base of the pilot, prior to hydrogen injection, comprised the following: Mach number, 3.18; static pressure, 6.9 psia; and static temperature, 1016°R.

For a specified fuel flow rate, the local mass flux ratios $\lambda$ at each pilot injector site could be calculated, and the combustion-induced flow deflection $\theta$ estimated from Fig. 9, reproduced from Ref. 5. The shock waves developed in response to the flow deflections were sketched on drawings of the combustor planform as shown in Fig. 10, enabling comparisons with the experimentally acquired pressures to be made. In this figure, the dashed parabola-like curves are the loci of the intersections with the ramp or cowl surface of the incident conical shock waves emanating from the individual burning jets located on the opposite surface. The solid, linear waves are those induced on the surface on which they are shown, and the dashed straight lines are the boundaries of the fuel–air mixing regions. The shock waves generated by the interactions between the combustor-entrance airflow and the fuel injectors are omitted in Fig. 10 for clarity.

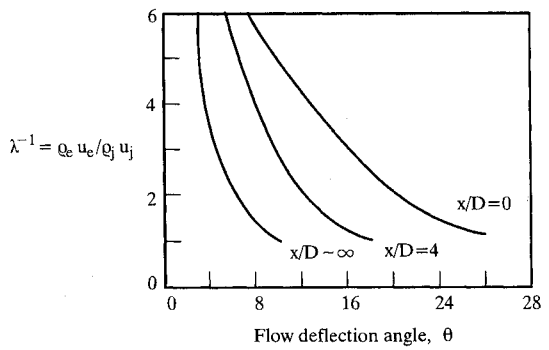


**Fig. 9 Flow deflection angles vs mass flux ratio.**

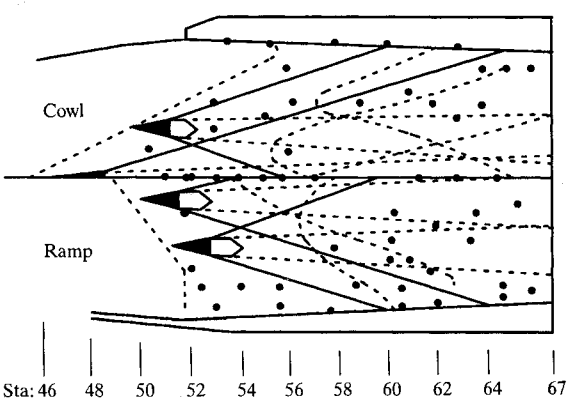


**Fig. 10 Loci of pilot shock-wave intersections on cowl and ramp.**

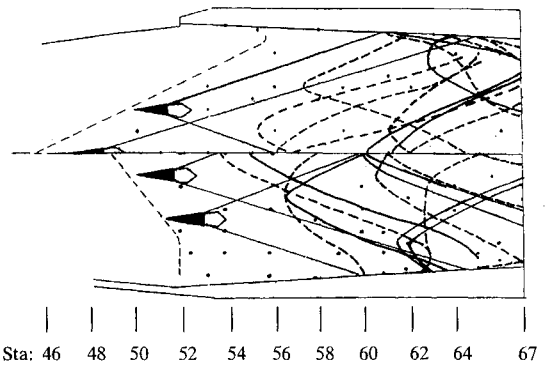


**Fig. 11 Loci of incident shock-wave intersections.**

Subsequent to defining the shock-wave intersections traced by the pilot–fuel combustion, and using the experimental data to verify the predicted pressure rises, the next set, i.e., secondary or strut-type, of fuel injection sites was selected. Locations downstream from the intersections of two pilot-combustion-induced shock waves were chosen to take advantage of the favorably high static pressures and temperatures induced there by the pilot-fuel combustion. These sites were thus located between the pilot diffusion flames, resulting in the delivery of fuel-free air to the fuel introduced there. Using the calculated local conditions at these selected sites, an estimate of the pressure rise that could be anticipated for various fuel flow rates was made. Experiments were again performed with this complement of fuel injectors and measured pressure data were compared with predicted pressure rises based on the analysis described below. Intersections with the surfaces of shock waves produced by this second set of fuel injectors were plotted on the combustor planform. Subsequent injection sites were added in similar fashion, i.e., analysis of the data from combustion experiments following injector installation, etc., yielding the full set of incident shock-wave intersections as shown in Fig. 11, until satisfactory stoichiometric operation of the engine without inlet interaction was achieved.

### Process Models

The test data analysis was based on the two-dimensional boundary-layer analysis formulated by Edelman.[5] In this treatment, the mixing process is assumed to be governed by the rate of diffusion normal to the main flow direction. The process itself is described using a parabolic boundary-layer equation system. Phenomenologically, the maximum heat release is assumed to occur along the surface of fuel–air stoichiometry, viz., the maximum temperature line. During the simultaneous heat release and density decrease, the flow expands outward, producing a "thermal compression" wave that propagates into the external flow. Figure 9, extracted from this reference, was used to predict the pressure rise to be expected to occur as a consequence of the combustion of injected hydrogen. The mass flux ratio $\lambda$ was calculated based on the hydrogen jet (subscript $j$) properties and the local airflow (subscript $e$) properties upstream from the injection location. From Fig. 9, the local flow deflection angle $\theta$ corresponding to the calculated mass flux ratio was obtained. Usually, the far-field flow deflections, i.e., corresponding to $x/D \approx \infty$ were used to determine the pressure rise across the combustion-induced shock wave and the shock-wave angle.

The pressure rises at various locations influenced by the conjunction of shock waves were estimated by "stepping" through the wave fields shown in Figs. 10 and 11. Consider the simplified five injection-site scheme shown in Fig. 12 in which only the compression waves induced through combustion are shown. In this figure, injection sites A, B, and C are placed on the ramp or lower surface at the combustor en-

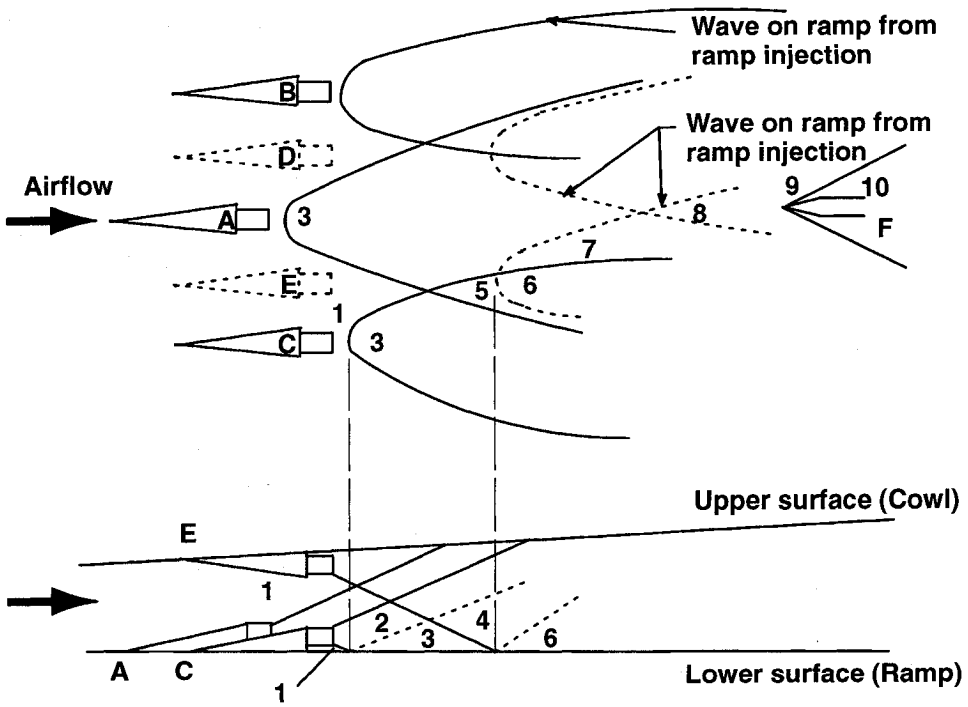


Fig. 12 Simplified five-injector flowfield. (Plan view at top and elevation.)

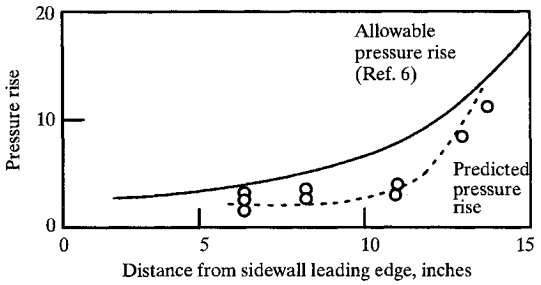


Fig. 13 Sidewall boundary-layer separation criterion.

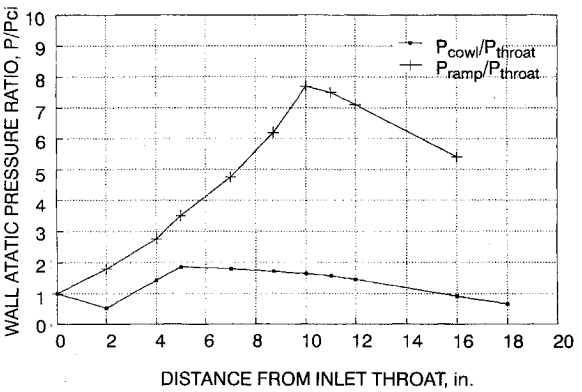


Fig. 14 Centerline axial wall pressure distribution.

trance, and sites D and E are on the cowl or upper surface. Waves intersecting the ramp and generated by combustion at site A are shown as solid lines. Waves intersecting the ramp and generated by combustion at site D are shown as dashed lines, etc. Assuming that the upstream flow conditions, the injected fuel flows, and the injector geometries are identical at each injection site, then fuel injection and combustion induce, everywhere, e.g., an initial pressure rise of 10%. That is, the pressure ratio across the first wave is $P_2/P_1 = 1.10$. Consequently, the pressure ratio behind the reflected wave is approximately

$$P_3/P_1 = P_3/P_2 \times P_2/P_1 = (P_2/P_1)^2 \quad (1)$$

$$P_4/P_1 \approx (P_2/P_1)^2 \times P_3/P_1 = (P_2/P_1)^4 \quad (2)$$

The addition of a fuel injector, e.g., labeled F in Fig. 12, results in the development of oblique shock waves characterized by a pressure ratio $P_{10}/P_9$, calculated in terms of the local Mach number $M_9$, and the injector geometry. The pressure rise induced by combustion at this site is then determined on the basis of the local mass flux ratio. Using these approximations, and disregarding the effect of the combustor cross-sectional area variation on the local pressures, one may "step through" the entire flowfield.

The extent to which the hydrogen, delivered by a group of fuel injectors, burned at a specific equivalence ratio was estimated by comparing the actual pressure rises attained during a combustion experiment at several affected pressure taps with the predicted pressure rises for those tap locations. Supplementing the analysis based on Ref. 5, it was found that the pressure rise $P_2/P_1$, induced by the combustion of fuel at an injector equivalence ratio $\phi$, could be expressed by the relationship:

$$P_2/P_1 = 1 + 22.5\phi \quad (3)$$

For example, $\phi = 0.01$ would yield a pressure rise of approximately 1.23. Using an influence coefficient $K$, a pressure tap influenced by the combustion of fuel from two injection sites, $a$ and $b$ would experience an overall pressure rise

$$p_{ab} = K_a(p_a) \times K_b(p_b) \quad (4)$$

where $p = P_2/P_1$. Through simultaneous solution for two appropriate injection sites, the values of $K_i$, the amount of fuel burned at each injection site, $i$ could be estimated.

To avoid local flow conditions during combustion that could lead to incipient separation of the boundary layer with the accompanying potential for a combustor–inlet interaction, a boundary-layer separation criterion found in Ref. 6 was applied to aid in the placement of fuel injection sites. Owing to

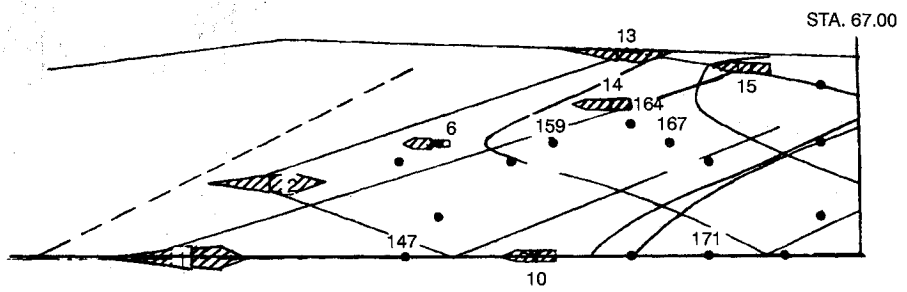


| $P_{tap}$ | Predicted | Measured | Predicted | Measured | Predicted | Measured |
|---|---|---|---|---|---|---|
| 147 | 1.14 | 1.12 | 1.92 | 2.46 | 1.72 | 2.58 |
| 159 | 1.30 | 1.18 | 2.28 | 2.22 | 2.52 | 2.58 |
| 164 | 1.19 | 1.03 | 3.45 | 3.40 | 5.30 | 5.70 |
| 167 | 1.36 | 1.27 | 3.45 | 3.40 | 5.30 | 5.15 |
| 171 | 1.36 | 1.35 | 1.19 | 1.13 | 1.66 | 1.21 |
| INJ. NRS. 1, 2, 4, 5 $\phi = 0.20$ | | | 6,8 $\phi = 0.40$ | | 10, 11, 12, 13, 14, 15 $\phi = 0.75$ | |

**Fig. 15 Cowl combustion-pressure rises at indicated pressure taps.**

the tendency for focusing of the compression waves to occur along the sidewalls of the combustor, the maximum pressure rises, and thus, the greatest tendency to separate the boundary layer would occur there. As a consequence, the sidewall pressure distribution was used to assess the propensity for separation to occur. Based on the calculated shock-wave intersections, pressure rises at various locations along the sidewall were estimated. These were compared, as shown in Fig. 13, with axial pressure distributions calculated using the approach from Ref. 6, to provide a criterion for maximum fuel addition.

### Experimental Results

A typical wall static-pressure distribution recorded during a high equivalence-ratio combustion test is presented in Fig. 14. The data comprise centerline distributions for the cowl and the ramp, normalized with respect to the ramp and cowl inlet-throat pressures, respectively. Note the significant differences between the levels measured on the cowl and ramp. Significantly greater compression occurs on the ramp side, as one might expect to observe based on the geometric differences between the ramp and cowl surfaces of the combustor (Fig. 6).

Some comparisons between the predicted and measured pressure rises induced by combustion on the cowl surface at overall equivalence ratios of 0.20, 0.40, and 0.75 are shown in Fig. 15. Satisfactory agreement between the predicted and measured cowl pressure increases was obtained at the pressure tap locations identified in the figure for fuel delivered at equivalence ratios, $\phi = 0.20$, 0.40, and 0.75 from the injectors indicated. A regression analysis yielded a determination coefficient for this comparison of 0.95. A similar analysis of the data for the ramp yielded poorer agreement with $R^2 = 0.84$.

The impulse increments $\Delta F/W$, measured during various phases of the combustor development, are shown in Fig. 16. The full complement of pilot and fuel injectors was installed in four steps, as follows: injectors 1, 2, 4, and 5; injectors 6 and 8; injectors 10–15; injector 9. Both nitrogen purge and hydrogen combustion data were acquired during each of these steps, and the highest performance levels attained during this process are represented by the data shown in Fig. 16. The target equivalence ratio for each of the seven pilot fuel injectors was between 0.02–0.04. With only these injectors installed, data were acquired for an overall equivalence ratio up to approximately 0.32, corresponding to an injector equivalence ratio of 0.045. When a second set, viz., the strut-type, of injectors was added, a higher thrust level was developed,

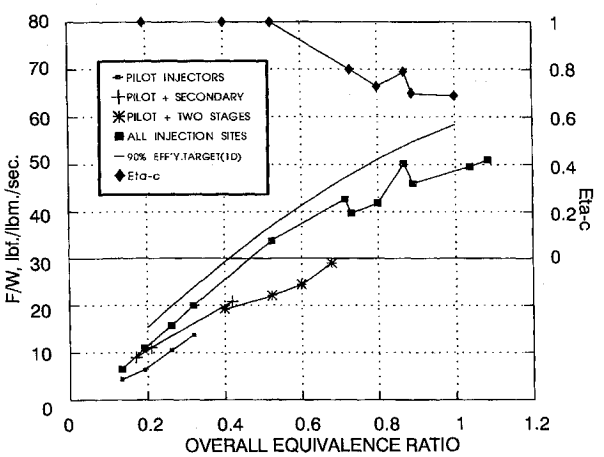


**Fig. 16 Module *F/W* data.**

even at the lower equivalence ratios, perhaps indicating an effect on the mixing and combustion processes of the interaction between the existing wave structure and the added fuel. The data shown for all of the injection sites active have been adjusted to account for the thrust produced by injector purge flow, and thus, represent the actual thrust levels, which are compared with the target thrust levels calculated for a combustion efficiency of 90%. The lower-thrust data, shown for the earlier injector development stages, are uncorrected, owing to the inability of the author to retrieve the purge data.

A cycle analysis, using the Johns Hopkins RJPA code,[7] was performed during the preparation of this document to evaluate the correspondence between the wall static pressure rise data and the thrust data, both of which were extracted from notes and reports that were more than 25 years old. The freestream conditions for the engine inlet were as follows: Mach number, 5.73; static pressure, 0.43 psia; total pressure, 684 psia; and total temperature, 2751°R.

For a freestream capture area of 94 in.$^2$ and an inlet contraction ratio of 3.92, the following inlet throat conditions were calculated: Mach number, 3.57; static pressure, 4.08 psia; total pressure, 411 psia; static temperature, 827°R; and capture weight flow, 10.01 lbm/s.

These inlet throat values compare favorably with the measured levels cited earlier, although the weight flow rate is slightly less than 10.2 lbm/s, the flow rate originally deduced

for the engine through calibration tests. The analysis was performed for test results obtained at an equivalence ratio of 0.75, for which a combustion efficiency of 73% and an internal specific thrust, $F/W$ of 37.6 lbf/lbm/s were originally determined, based on an air weight flow rate of 10.2 lbm/s. The cycle analysis, performed with no-entropy limit constraint, yielded, for a pressure rise of 5.7 and a 100% nozzle efficiency, a specific thrust of 39.5 lbf/lbm/s, and a specific impulse of 1783 lbf-s/lbm.

## Concluding Remarks

This investigation resulted in the development of a scramjet engine concept using fuel-injection tailoring to avoid the onset of deleterious combustor–inlet interactions. The measured wall static pressure distributions indicated that the combustor-flow Mach numbers remained supersonic during the combustion process, effectively corresponding to hypersonic-combustion operation of the combustor. A procedure was formulated and applied for the selection of fuel injection sites. The appropriateness of those sites was assessed using local wall static pressure data to estimate local combustion efficiencies. An available boundary-layer separation criterion was used to limit fuel introduction at specific sites to levels that would lessen the tendency for inlet interactions to occur. Comparison of the results obtained during the original investigations with those obtained using a current cycle analysis applied to the original geometry and original test conditions yielded satisfactory correspondence between the two data sets.

Clearly, a suitable computational fluid dynamics analysis can be used for combustor analysis, and possibly as a design tool for fuel injection site selection in scramjet combustors. The method outlined in this document may, however, with some modification, provide an approach to understanding the experimental data and to enable rapid diagnoses of combustor behavior.

## Acknowledgments

The support of the United Technologies Research Center in the preparation of this paper is gratefully acknowledged. This article is dedicated to the memories of E. Sanlorenzo and A. Ferri who provided both the incentive to do the work described in the original report and guidance in the formulation of the procedure. Thanks are due also to R. B. Edelman for providing some of the fundamental concepts used and for stimulating discussions regarding their application at the time of the investigation, and to Eliahu Reiss for his assistance with the extensive hand calculations.

## References

[1]Brown, M. L., and Maxwell, R. L., *Scramjet Incremental Flight Test Program*, Vol. 1, Summary, Air Force Aero Propulsion Lab. TR-67-112, The Marquardt Corp., Summary Rept., Rept. 6131, Van Nuys, CA, Feb. 1968.

[2]Ferri, A., "Mixing Controlled Supersonic Combustion," *Annual Review of Fluid Mechanics*, Vol. 5, 1973, pp. 301–338.

[3]Anderson, G., Kumar, A., and Erdos, J., "Progress in Hypersonic Combustion Technology with Computation and Experiment," AIAA Paper 90-5254, Oct. 1990.

[4]Peschke, W. T., and Reiss, E., "Diffusion Controlled Supersonic Combustion, Analysis and Design of Combustors," General Applied Science Labs. TR 672, Westbury, NY, Nov. 1967.

[5]Edelman, R. B., "Diffusion Controlled Combustion for Scramjet Application, Part I, Analysis and Results of Calculations," General Applied Science Labs. TR 569, Westbury, NY, Dec. 1965.

[6]Kuehn, D. M., "Experimental Investigation of the Pressure Rise Required for the Incipient Separation of Turbulent Boundary Layers in Two-Dimensional Supersonic Flow," NASA Memo 1-21-594, Feb. 1959.

[7]Pandolfini, P., "Instructions for Using Ramjet Performance Analysis (RJPA) IBM-PC Version 1.0," Johns Hopkins Univ., Applied Physics Lab., JHU/APLNASP-86-2, Laurel, MD, Nov. 1986.